Investigating the Impact of Solid-Electrolyte Interface on Dendrite Formation: A Case Study Based on Zinc Metal Electrodes

D. Gregory[1], C. Britten[2], K. B. Walters[2,] and Ö. Ö. Çapraz[1]

[1]The School of Chemical Engineering, Oklahoma State University, Stillwater, OK 74074

[2]Ralph E. Martin Department of Chemical Engineering, University of Arkansas, Fayetteville, AR 72701

ABSTRACT

The formation of dendrites is the bottleneck to harvest the high theoretical capacities of metal anodes such as Li, Na, Mg, and Zn batteries. The critical current density, interfacial instabilities, and the characteristic of the solid-electrolyte interface (SEI) layer play a major role in the formation mechanisms of dendrites. In this study, we investigated the impact of the SEI layer on the electroplating of zinc metals in organic and aqueous electrolytes by using electrochemical techniques coupled with electron microscopy and X-ray photoelectron spectroscopy. First, the electrochemical response of Zn plating in organic or aqueous electrolytes was compared with the ones for Li and Na metal plating by using analogous perchlorate salt dissolved in the same organic solvent. Under similar charge conditions, the cycle life of the metal electrodes was longer in the order of Zn (aqueous) > Li > Zn (organic) > Na. The impact of the SEI layer is then investigated by electroplating Zn in aqueous for 20 cycles, and then switching it to organic electrolytes and vice versa. In organic electrolytes, the cycle life of the PAO-Zinc is almost three-fold longer than the as-received zinc electrodes. PAO stands for pre-cycled in aqueous electrolyte for twenty times. Overall, our study demonstrated the impact of surface chemistry and morphology on the formation of Zn dendrites. The methodology established here can be used to study the impact of electrolyte salt and additives on the formation of dendrites on metal electrodes.

Key Words: Dendrite, solid-electrolyte interface, metal batteries, interfacial kinetics, Zinc

1. INTRODUCTION

The Li-ion battery has been a tremendous success since its commercialization by Sony in 1991 with applications in portable electronics, renewable energy storage, and electric vehicles[1]. However, the practical charge storage capacity of the intercalation electrodes commonly used in commercial lithium-ion batteries is approaching its theoretical limit[2,3]. This imposes a restriction on the energy density of lithium-ion batteries and impedes progress towards developing batteries with higher energy density. One potential solution is to replace the graphite anode with a metal electrode. Instead of intercalating ions into a host structure, charge storage on metal anodes occurs through deposition/dissolution of metal ions on the electrode surface. With the elimination of an inert host structure, metal anodes feature much higher theoretical energy densities than traditional anodes. For example, the theoretical capacity of a Li metal anode (3860 mAh g^{-1}) is almost 10 times higher than graphite (372 mAh g^{-1}). Beyond Li batteries, sodium (1165 mAh g^{-1}) and zinc (820 mAh g^{-1}) anodes feature high specific capacities as well. Additionally, the metal anode provides a source of metal ions to a variety of battery geometries such as metal-air and metal-sulfur batteries which have very high theoretical capacities in comparison with metal-ion batteries.

Unfortunately, utilization of metal anodes in rechargeable metal batteries is limited due to severe performance loss and safety issues associated with the formation of dendrites. Uneven electrodeposition of the metal ions over the surface of the metal anode leads to the formation of dendrites[4–6]. These dendrites present a potential safety hazard for inflammable organic electrolytes because, over repeated charge/discharge cycles, they can grow through the electrolyte and cause an internal short-circuit by contacting with the cathode[7]. Solid-electrolyte interphase (SEI) plays a crucial role in the electrodeposition of metal ions. These SEI layers forms due to highly negative electrochemical potentials of metallic anodes which are higher than the lowest unoccupied molecular orbital (LUMO) of the electrolyte[8,9]. Even the small surface roughness on the SEI layers can cause distortion transportation of ions, leading to non-uniform metal ion electroplating[10]. The formation of new SEI layers continues unless the electrode is passivated by a desirable SEI layer that prevents electron transfer between the anode and the electrolyte. However, if the SEI is not elastic enough, it can break down during lateral expansion of metal volume during electrodeposition, causing the exposure of the fresh metal surface to the electrolyte and therefore formation of new SEI layers. Also, during the stripping of metal ions from the dendrites, the

process may lead to the generation of "death metal" by physically disconnected from the bulk electrode by the dissolution of metal from the base of the dendrite[11–13]. The combination of continuously forming SEI layers and production of "dead" metal lead to low Coulombic efficiencies in metal anode batteries and limits their reversibility and cycle life[14].

Various solutions to the dendrite problem have been proposed including artificial SEI layers[15–19], electrolyte additives[20–24], solid-state electrolytes[25–28], 3D current collectors[29–31], pulsed current charging/discharging protocols[32], and rapid oxidation / reduction[33]. However, a better understanding of the mechanism behind the dendrite formation is required to develop effective strategies to overcome the dendrite problem in the metal anodes. Recently, Dasgupta and his group utilized operando microscopy to correlate voltage trace shape and morphology changes of the electrode during galvanostatic plating/stripping using symmetric Li cells[34–36]. This explanation was later extended to account for further voltage trace evolution over extended cycling and is a valuable resource for interpreting symmetric cell data[37]. Mandl et al utilized a similar approach to correlate morphology and voltage profiles for sodium anodes[13]. In all of these cases, the nature of the SEI layer formed on the anode surface played an important role in the performance and resulting overpotentials for the cells tested.

In this study, our objective is to understand the impact of the solid-electrolyte interface on the electroplating / stripping performance of Zn metal anodes. To achieve it, we first investigate the voltage profiles for three different metals (Li, Na, Zn) in symmetric cell configuration using the same salt anions and organic electrolytes. Lithium and sodium are both highly chemically reactive metals and cannot be used with aqueous electrolytes. On the other hand, Zn metal can be used in both aqueous and organic electrolytes. This is a very beneficial feature, as Zn metal will not form an SEI layer containing organic species in aqueous electrolytes which allows for determining the influence of organic species in SEI layers on voltage trace evolution and long-term cycling performance. Then, we investigate the impact of the SEI layers forms in organic and aqueous electrolytes by preparing pre-cycled zinc samples. Electrochemical performance and morphological changes on the surface of the Zinc electrodes were characterized by performing electrochemical techniques, electrochemical impedance spectroscopy (EIS), scanning electron microscopy (SEM) with energy dispersive X-ray analysis (EDX), and X-ray photoelectron spectroscopy (XPS).

2. EXPERIMENTAL METHODS

Sample Preparation: Lithium (99.9% metal basis), sodium (99.9%, metal basis), and zinc metals (99.9% trace metals basis) were purchased from Alfa Aesar and Sigma Aldrich, respectively. The lithium and zinc metals were used as received. Na metals were prepared using the methodology described in our previous publication[38]. The sodium cubes were purchased in a mineral oil solution. They were cleaned with hexane in a glovebox to remove mineral oil. The cleaned sodium cubes were stored in a 1:1 (V: V) solution of ethylene carbonate (EC, anhydrous, 99%, Sigma Aldrich): dimethyl carbonate (DMC, anhydrous, >99%, Sigma Aldrich) inside the glove box. During symmetric cell assembly, the sodium cubes were removed from the storage solution, dried using a paper towel, and the exterior surface of the cubes comprised of an oxidized layer was cut off using a stainless-steel scalpel. The unoxidized, center cut piece was then placed in a plastic bag and rolled out into a thin film using a rolling pin.

Electrochemical Characterization: The electrochemical performance of Li, Na, and Zn metals was investigated by using symmetric cells. All symmetric cells utilizing organic electrolytes were assembled in an Ar-filled glovebox (H_2O and O_2 concentrations < 1 ppm). Celgard polyethylene separator was used for Li symmetric cells. Borosilicate glass fiber separator (Whatman GF/D was used for Na and Zn symmetric cells. The organic electrolyte was prepared by dissolving 1M $LiClO_4$, $NaClO_4$, or $Zn(ClO_4)_2$ in EC: DMC solvent for Li, Na, and Zn symmetric cells, respectively. Aqueous electrolytes were prepared by dissolving $Zn(ClO_4)_2$ in ultrapure water. Zinc electrodes cycled in aqueous electrolytes were prepared in the room environment. The electrochemical stripping and plating of metals were conducted by applying galvanostatic cycles at |1| mA cm^{-2} for 60 minutes. Electrochemical impedance spectroscopy (EIS) was conducted on the as-received and cycled cells using a Biologic potentiostat equipped with EC-EC-lab® acquisition software with an amplitude of 50 μA cm^{-2}.

Structural and Morphological Characterization: SEM images were acquired from an FEI Quanta 600 field emission gun ESEM with Bruker EDS and HKL EBSD. Coin cells were disassembled using an MTI disassembly die set inside a glovebox under an Ar atmosphere. Samples were transferred between the glovebox and the SEM chamber using a sealed SEM transfer container to minimize ambient air exposure. At the SEM, samples were transferred as quickly as possible between the SEM transfer module and SEM vacuum chamber to minimize sample contact with

oxygen or moisture in the air. Zinc electrodes cycled in aqueous electrolytes were dissembled in the room environment for characterization.

X-ray Photoelectron Spectroscopy Characterization: XPS data were collected using a Physical Electronics 5801 MultiTechnique system. All spectra were collected using a standard aluminum anode with an aluminum filament, an accelerating voltage of 15 kV, anode power of 300 W, an analysis area of 0.6 mm x 2.0 mm, and a takeoff angle of 45°. Survey spectra were collected using a pass energy of 187.85 eV with a step size of 0.8 eV. High-resolution spectra were collected using a pass energy of 58.7 eV with a step size of 0.125 eV. All samples were fixed to the sample stage using carbon tape inside a nitrogen-filled glovebox (H_2O and O_2 concentrations < 1 ppm) along with a sheet of gold foil to align the stage prior to analysis. The sample stage was transferred to the instrument using a sealed transfer vessel to prevent atmospheric exposure. Samples were held under vacuum in the introduction chamber (ca. 10^{-7} torr) for at least one hour prior to introduction to the main chamber to outgas volatile compounds.

3. RESULTS AND DISCUSSION

3.1. Galvanostatic Cycling Profiles of Li, Na, and Zn Metals: Electrochemical performance of the Li, Na, and Zn metals were characterized using symmetric cells during charge/discharge galvanostatic cycles. The cycle is defined as one stripping/plating process of metal ions on the electrode. Between each charge-discharge cycle, the cell was in open circuit condition (no current applied) for 3 minutes. To minimize the role of anionic electrolyte species on the plating/stripping behavior, an analogous perchlorate salt ($LiClO_4$, $NaClO_4$, or $Zn(ClO_4)_2$) - containing electrolytes were used in all experiments. Li and Na symmetrical cells were only tested in ethylene carbonate: dimethyl carbonate (EC: DMC) organic solvent. However, the plating/stripping behavior of Zn anode was characterized in EC: DMC organic solvent and aqueous electrolyte. EC: DMC mixture is chosen as a model organic carbonate solvent because of its rich literature on Li and Na plating in this solvent[5,39]. Resistance on the as-received Li, Na, and Zn cells in either organic or aqueous electrolytes was measured using impedance spectroscopy (Supp, Fig 1). Symmetrical as-received Zn cell in an aqueous electrolyte demonstrates the lowest resistance. Large resistance was recorded for as-received Zn and Na cells in organic electrolytes.

Figure 1 demonstrates the voltage profile of Li vs Li, Na vs Na, and Zn vs Zn symmetrical cells during plating / stripping at ± 1 mA/cm^2 current density. The potential hysteresis in the Li vs

Li symmetrical cell initially reduced gradually to 0.114V around 50 cycles. After that, the potential hysteresis continuously increased up to 0.290V at around 200 cycles before short-circuiting. In the case of Na plating, the potential hysteresis dramatically increased before reaching the cut-off voltage of 1V on the 36th cycle. The potential hysteresis in the Zn vs Zn symmetrical cell cycled in the organic electrolyte started around 0.3V and reduced to about 0.17V after 10 cycles. The hysteresis was almost constant until around the 65th cycle and the cell short-circuited around the 90th cycle. On the other hand, in the aqueous electrolyte, the potential hysteresis reduced from 0.1V to 0.07V within the first 10 cycles. The hysteresis was almost constant around 0.05V until the cell was short-circuited around the 225th cycle. Overall, when symmetrical Li, Na, and Zn cells were cycled under the same current density and using analogous perchlorate salt, the cycle life of the metal electrodes was longer in the order of Li > Zn > Na. The cycle life of the Zinc metal electrodes cycled in aqueous electrolytes was almost two-times longer than the ones in organic electrolytes.

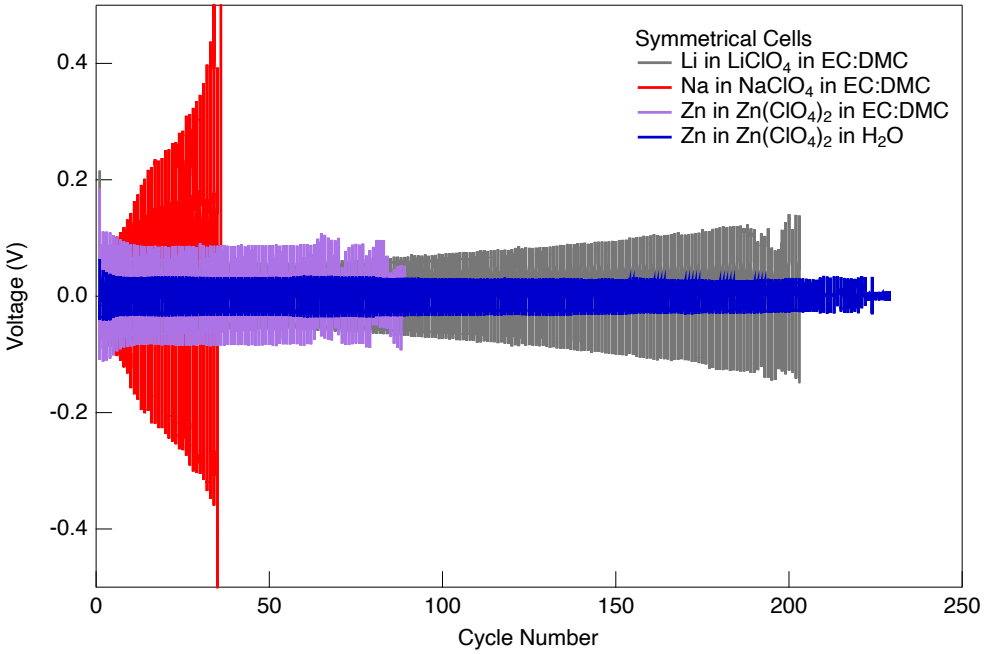

Figure 1: Voltage profile of Li vs Li, Na vs Na and Zn vs Zn symmetrical cells during plating / stripping at ±1 mA/cm^2 current density

3.2 Voltage Profile Observations: Voltage profiles during plating/stripping of metal electrodes provide information about the morphological changes on the metal electrode. Previous research efforts have linked the evolution of the voltage profiles in Li and Na symmetric cells during galvanostatic cycling to morphological changes on the electrode surface[13,36]. The voltage profiles

in Zn symmetrical cells, cycled in both aqueous and organic electrolytes, were compared with the voltage profiles in Li and Na symmetrical cells.

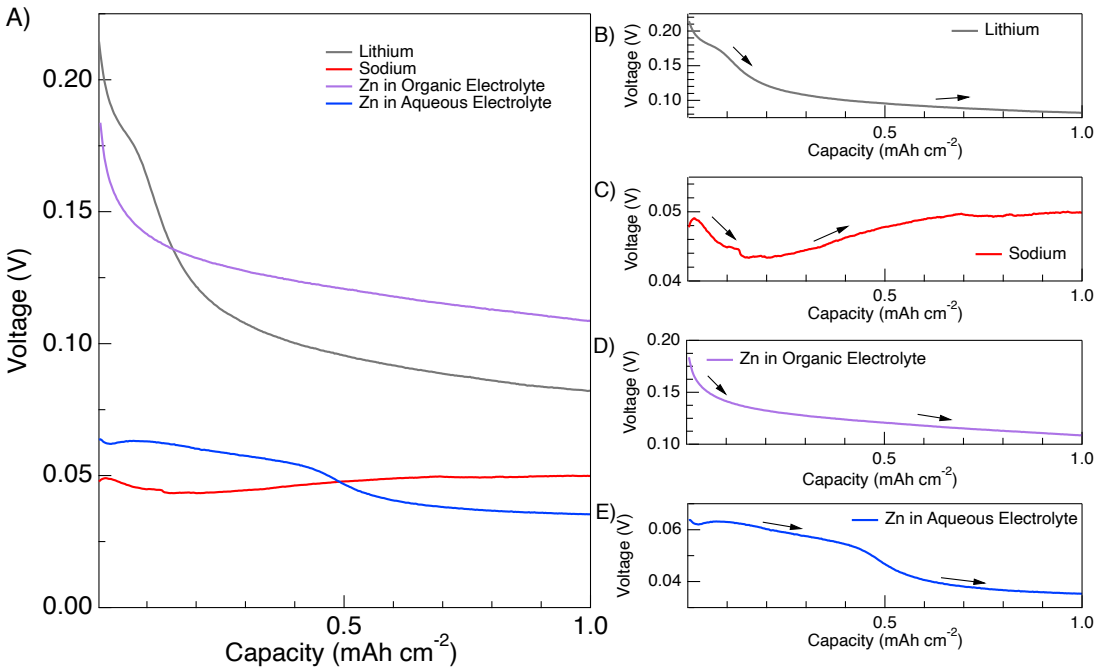

Figure 2: 1st galvanostatic half-cycle voltage profiles at 1 mA cm^{-2}. A) Comparison between Li, Na, Zn in organic electrolyte, and Zn in aqueous electrolyte symmetric cell. Voltage profiles for B) Li, C) Na, D) organic Zn, and E), aqueous Zn

First charge: Initially, the symmetric battery cells consist of as-received metal electrodes. Although both electrodes are identical before cycling, to avoid confusion, the electrode is called a counter electrode where metal ions were generated at its surface during the first charge. The other electrode is called a working electrode where generated metal ions are plated on its surface during the first charge. Li plating on the working electrode began with a maximum cell voltage of 0.214 V and it gradually decayed to 0.082 V at the end of the first charge cycle. The shape of the voltage evolution during the first lithium plating on the as-received Li metal electrode is very similar to the previous Li symmetric cells studies in the literature[40,41]. Dasgupta and his group provided a detailed correlation between the transient morphological changes on the Li metal electrodes and the voltage profile for each plating/stripping cycle using in-situ optical microscopy[36]. According to their studies, the initial maximum is correlated with overcoming the energy barrier associated with the nucleation of Li onto the cathode surface. A decay in the overpotential is then observed

as the cathodic process switches from nucleating new Li deposits to plating Li on the existing deposits, a more kinetically favored process requiring lower overpotentials[36]. The voltage profile during the first charge cycle in symmetric Zn cell cycled in organic electrolyte shows very similar behavior with the Li symmetric cell. The initial voltage of the cell was 0.184 V and it reduced to 0.109 V. The initial voltage in the symmetrical Zn cell in an aqueous electrolyte was lower compared to the zinc cell cycled in an organic electrolyte. The voltage of Zn cell in an aqueous electrolyte slowly decreased from 0.064 to 0.035 V. In the case of Na, the voltage initially dropped from 0.048 to 0.043 V within the initial 10 minutes of the charge cycle, and then it slowly increased to 0.050 V by the end of the charge cycle. The shape of the voltage evolution in the first discharge is similar in behavior with the subsequent charge and discharge cycles.

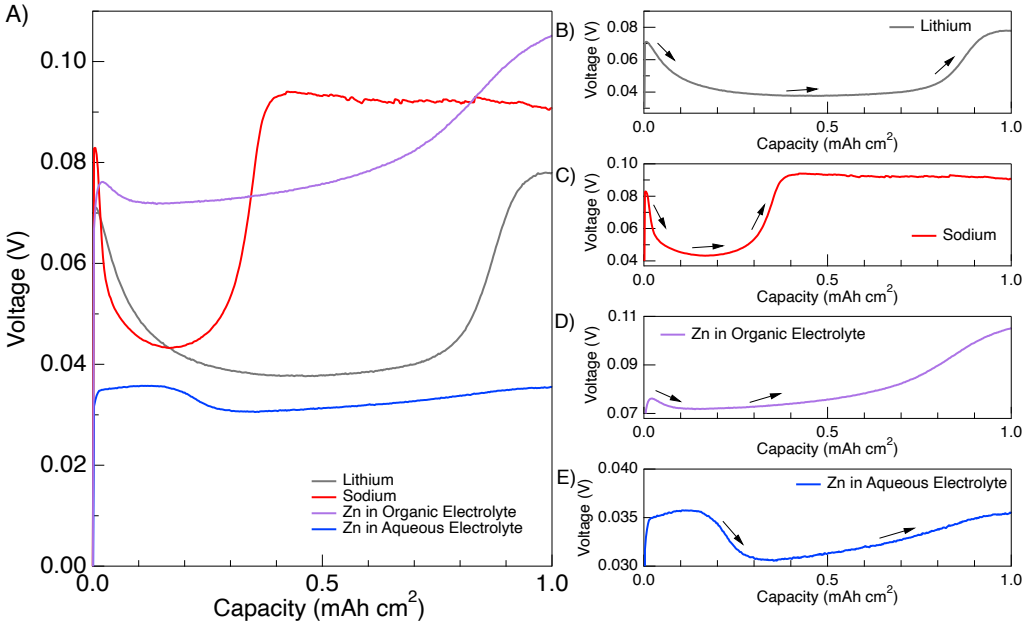

Figure 3: Fifth charge cycle voltage profiles at 1 mA cm^{-2}. A) Comparison between Li, Na, Zn in organic electrolyte, and Zn in aqueous electrolyte symmetric cell. Voltage profiles for B) Li, C) Na, D) organic Zn, and E), aqueous Zn

***Fifth Charge*:** During the fifth charge cycle, the metal ions are generated on the previously plated counter electrode, and they are plated on the working electrode. As the sign of the applied constant current was switched from negative (fourth discharge cycle) to positive (fifth charge cycle), the voltage of the symmetric cells jumped to 0.071 V, 0.083 V, 0.076 V, and 0.035 V for Li, Na, Zn in organic electrolyte and Zn in aqueous electrolyte cells, respectively.

After the initial increase, the voltage of the Li symmetric cell decreased to local minima, 0.038 V within 28 minutes of applied current. From this minimum, the voltage increases again to a maximum value of 0.078 V where it plateaus after 58.5 minutes of applied current. Similar to the first charge cycle, the initial maximum overpotential is required to overcome the nucleation potential on the surface of the counter electrode. Then, the potential gradually decreases as the plating mechanism switches from nucleation to growth of Li deposits[36]. Unlike the first charge, Li metals are stripped off from the dendritic depositions on the working electrode. Eventually, Li ions can no longer be generated from the dendritic deposits. Optical microscopy studies showed some of the dendrites on the counter electrode are either disconnected from the surface of the electrode or become electrochemically inactive[34,36]. As a result, Li begins to be stripped off from the bulk surface of the working electrode. This point is correlated with the localized minima in the voltage profile. From this point, the location of the stripped Li will begin to transfer from the bulk surface to the newly created pits on the surface. The transition from bulk stripping to pit stripping is represented through the increase in overpotential. In the case of Na plating/stripping in Na symmetric cell, the initial voltage peak of 0.0828 V is followed by a sharp drop in the voltage to a value of 0.043 V within the first 10 minutes. A notable difference in the two alkali metals is that the cell voltage reaches the first voltage plateau much quicker in the Na symmetric cell than the Li. After the plateau, the voltage increased to its second peak value of 0.094 V after 25 minutes before plateauing at 0.090 V. A similar observation was recorded by Mandl et al in their symmetric cells alongside in-situ optical microscopy video footage[13]. The differences in voltage evolution between Na and Li symmetric cells were associated with a larger amount of "inactive" Na being formed than "inactive" Li under similar conditions thereby providing less active metal to strip from the electrochemically active dendrites[13]. After the 2nd voltage peak, voltage gradually decreased in the Na symmetrical cell and it was associated with Na ions being extracted from the pitted areas. The Zn symmetrical cell cycled in organic electrolyte also displayed an analogous overall shape in its voltage trace. However, the first voltage peak is much less pronounced. There is a more gradual increase in overpotential to a final maximum value of 0.105 V.

In the case of symmetric Zn cell cycled in aqueous electrolyte, the first voltage peak was much broader than the voltage peaks in Li, Na, and Zn cells cycled in organic electrolyte eventually

reaching a value of 0.036 V after 6.5 minutes before decreasing. After the initial voltage peak, the evolution of voltage resembles metal electrodes cycled in organic electrolytes. Afterward, the voltage dropped to its minimum value, 0.031 V, and slowly increased up to 0.036 V at the end of the half-cycle. However, it is important to note that potential change from the initial peak to the plateau is only 0.005 V, similar to the organic zinc cell with a drop of 0.004 V, whereas potential drop from the initial peak to plateau in Li and Na symmetrical cells in the organic electrolyte is 0.033V and 0.040 V, respectively.

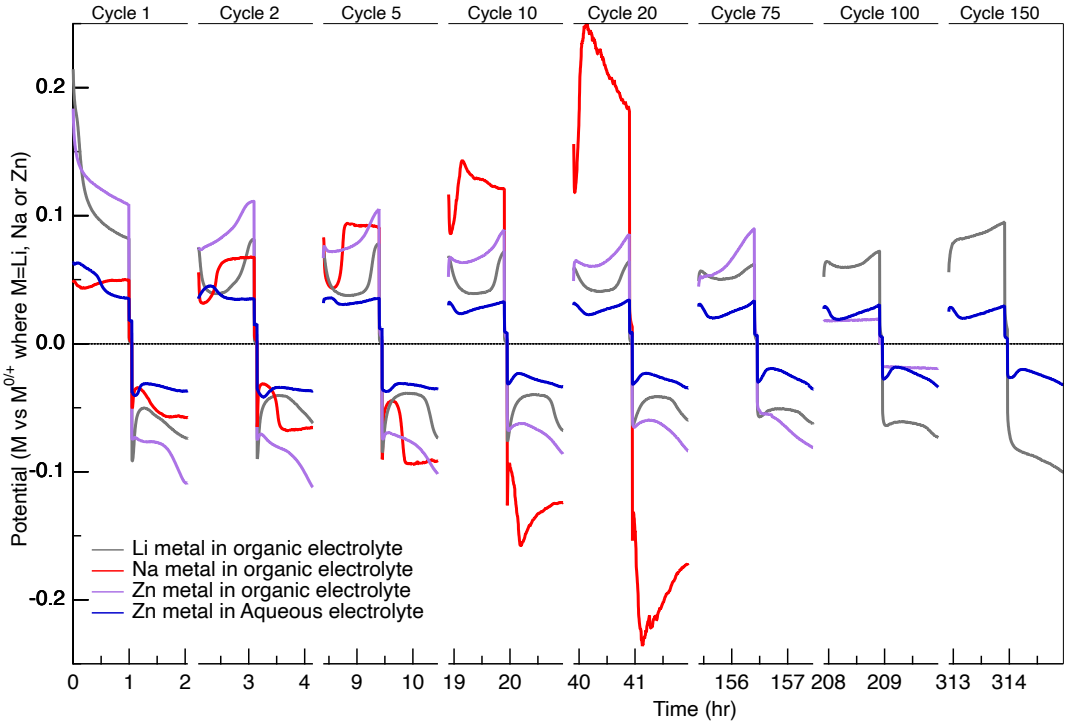

Figure 4: Galvanostatic cycling profiles from specific cycles for Li, Na, organic Zn, and aqueous Zn symmetric cells at 1 mA cm^{-2} showing the evolution of the voltage traces over extended cycling

Later Cycles: Figure 4 shows the voltage profiles in Li, Na, and Zn symmetrical cells from Figure 1 during their 1st, 2nd, 5th, 10th, 20th, 75th, 100th, and 150th cycles. A distinct evolution in the voltage trace for each cell can be observed over long cycling. In the Li symmetric cell, the voltage dipping between the two potential peaks becomes shallower over extended cycling. The minimum half-cycle voltage increased from 0.038 V in cycle 5 up to 0.052 V in cycle 100. An accompanying decrease in the first voltage peak from 0.071 V to 0.064 V and the second voltage peak from 0.078 V to 0.072 V is also observed between the 5th and 100th cycles. A decrease in cell polarization

during initial cycling is commonly reported in the literature and is attributed to the formation of higher surface area lithium deposits and lowered interfacial impedances[37]. Additionally, the initial peak broadened over extended cycling. Whereas the peak was reached within the first 10 seconds in the fifth cycle, it took 3 minutes before the local maximum was reached in cycle 100. Over further cycling, this voltage minimum disappears and the overall shape switches from peaking behavior to the arcing shape and increased overpotentials. This evolution was attributed to the accumulation of dead Li within the cell which imposes Li-ion mass transport limitations[37]. The switch from reaction kinetics limitations to mass transport-controlled behavior produced the more pronounced arcing behavior.

The voltage profile of the Na symmetric cell rapidly changed over cycling. The 2nd voltage peak occurred progressively earlier with extended cycling and the voltage dip between the two peaks shrunk. The 2nd peak occurred at the 25-minute mark in the fifth cycle, but only after 13.5 minutes in cycle 20. Furthermore, the magnitude of the 2nd voltage peak increased dramatically over cycling. In cycle 5, the maximum potential was 0.094 V; however, this value increased to 0.251 V in cycle 20. The organic zinc cell's voltage profile remains relatively constant over prolonged cycling. The most prominent difference lies in the magnitude of the first voltage peak. The initial voltage peak has a value of 0.076 V in the fifth cycle which decreases to 0.054 V in cycle 75. In the case of the aqueous zinc cell, the initially broad first peak progressively narrows after many cycles. With the narrowing of this peak, the voltage profile of the aqueous zinc cell begins to resemble the lithium cell more closely, with a narrow initial peak followed by a dip in voltage, a second maximum, and lastly a voltage plateau.

***Morphological Evolution of Zn electrode*:** Morphology evolutions on Zinc metal anode was investigated by using scanning electron microscopy after cycling in either aqueous or organic electrolytes. Figure 5A shows the morphology of the as-received Zinc metal electrode. When zinc is cycled in an aqueous electrolyte for twenty times, the needle-shaped dendrites were observed on the surface of the Zinc electrode (Fig 5 C and Supp. Fig 3). On the other hand, mossy-type dendrite shapes were detected when cycled in organic electrolytes (Fig 5G). In both electrolytes, the generation of pits was observed on the surface of the electrode due to the stripping of Zn from the metal surface (Fig 5B,F). Pits were easily identified on the surface of zinc after cycling in aqueous electrolytes for twenty times (Fig S4). However, when cycled in organic

electrolyte for twenty times, we could not find pits due to the formation of the cathode-electrolyte interface. Therefore, SEM image is taken after cycling Zinc in organic electrolyte for two cycles, and pit formation was detected clearly (Fig 5F).

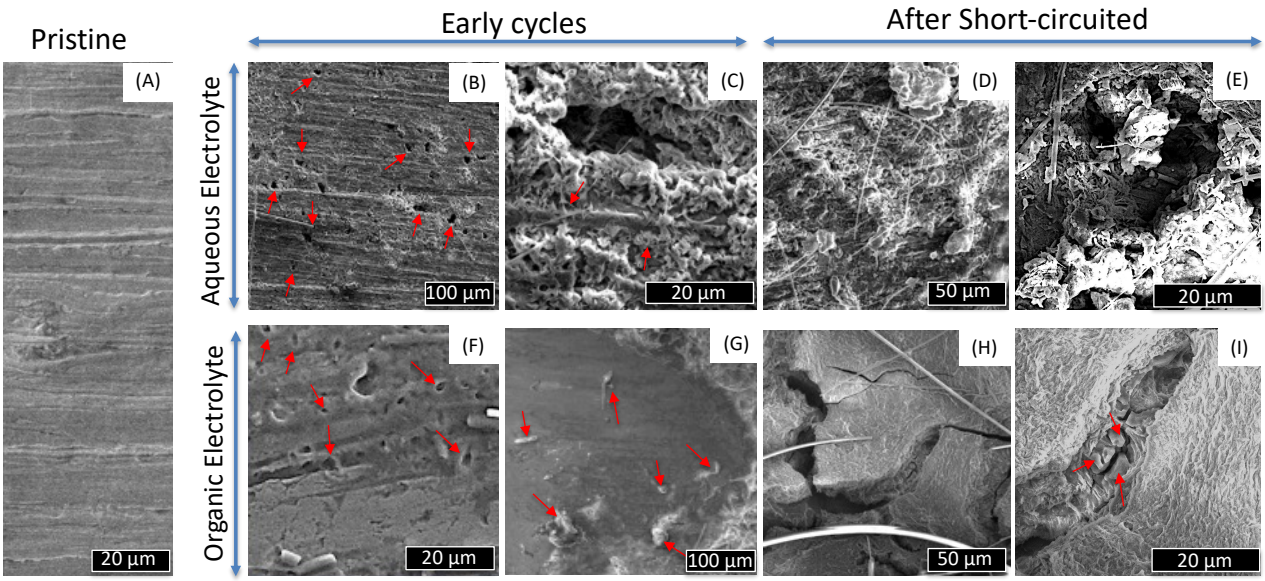

Figure 5: SEM images of (A) as-received Zn electrode, (B, C) Zn electrodes after 20 cycles in aqueous electrolyte, (D, E) Zn electrodes after short circuit in aqueous electrolyte, (F) Zn electrode cycled in organic electrolytes for 2 cycles, (G) Zn electrode cycled in organic electrolytes for 20 cycles, (H, I) Zn electrode after short circuited in organic electrolyte. Arrows demonstrated the representative morphologies such as pits (B and F) and dendrites (C, G, and I) in selected images.

We also compared the final morphology of the Zinc electrodes after symmetric cells were short-circuited in organic or aqueous electrolytes. In the case of aqueous electrolytes, the dendritic deposits and pits further progress, and a large number of dendritic deposits were captured on the electrode surface (Fig 5D,E). However, the surface of the Zinc electrode was covered by a thick layer of the solid-electrolyte interface when the electrode was cycled in the organic electrolytes (Fig 5H,I). Due to the volumetric expansion and contraction of the electrode during Zn plating/stripping, the SEI layer has fractured and large cracks are observed. Looking into these cracks reveals Zn dendrites growing up into the SEI layer. The presence of this pronounced SEI layer is one of the most obvious differences between the electrodes cycled in the two electrolytes. This is to be expected as organic species in the electrolytes decomposes at lower potential and forms solid-electrolyte interface (SEI) later on the anode surface.

The chemical composition of the zinc electrodes was examined via EDS analysis after cycling zinc in organic or aqueous electrolytes for twenty times. Cl was uniformly covered on the surface of the Zinc cycled in an organic electrolyte (Fig S2). However, Cl species were found on edge of the pits or surface of the dendrites when the zinc was cycled in an aqueous electrolyte (Fig S3 and S4). Ex-situ XPS analyses were performed for Zinc cycled in aqueous electrolyte for twenty times or zinc cycled in organic electrolyte for two times (Fig S5). In both cases, almost 20% of the surface chlorine is reduced to free chloride. Surface analysis by XPS of the Zn cycled in an aqueous electrolyte contains 11% Zn and 89% ZnCl. In comparison, after cycling only two times in organic electrolyte the surface composition of the zinc showed about 1.7% Zn and 98.3% ZnCl. This indicates a much thicker surface layer was formed in the organic electrolyte just after two cycles than cycling in aqueous electrolyte for twenty cycles. The thicker surface layer results in less penetration into bulk Zn metal during XPS analysis as a result.

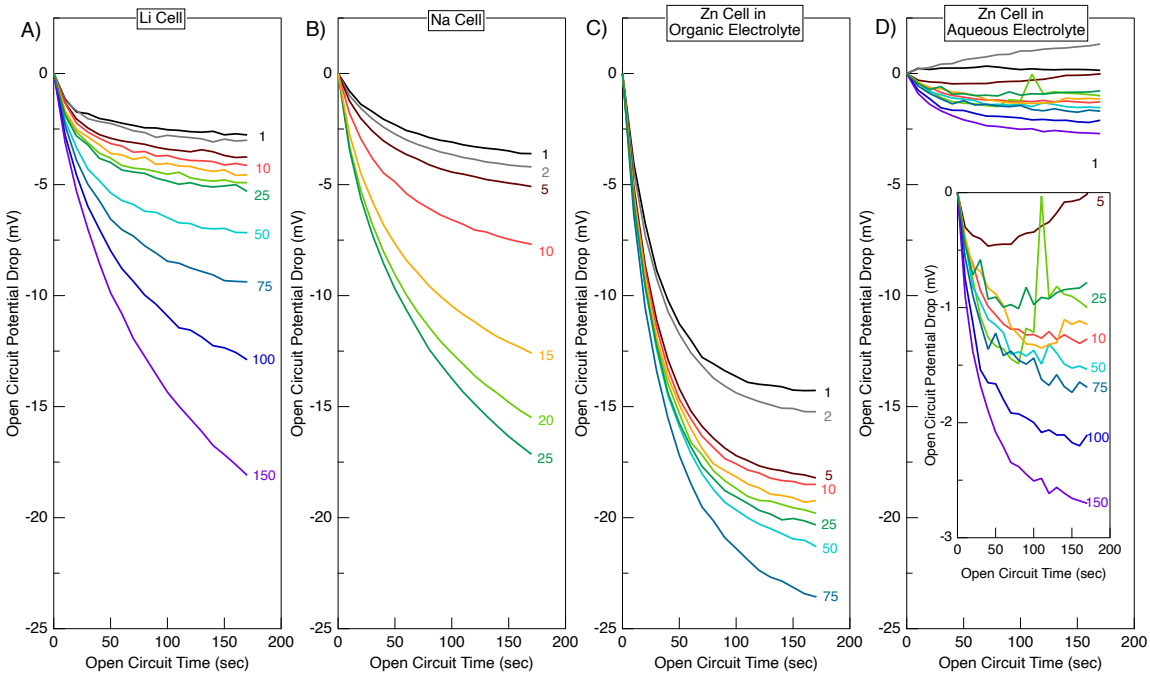

Figure 6: Open-circuit potential drops for selected cycles for A) Li, B) Na, C) Zn symmetric cells in organic electrolytes, and D) Zn symmetric cell in aqueous electrolyte.

Open Circuit Potentials: Between each plating/stripping half-cycle, a 3-minute open circuit rest period is employed to allow the concentration of ions across the cell to approach equilibrium. This allows each half-cycle to start with near-equilibrium conditions for the surface reaction at each

electrode. Metal ions are generated at one electrode and consumed at the other in the deposition/dissolution electron transfer reactions. The generation and consumption of metal ions at each electrode moves the concentration of ions away from equilibrium and introduces a concentration gradient across the cell. The severity of the concentration gradient depends on the effective diffusion coefficient of metal ions in the cell with greater mass-transport limitations inducing larger concentration gradients. As the interfacial concentration of metal ions at the surface of both electrodes changes, a larger overpotential is needed to drive the plating/stripping processes according to the equation[42]

$$U - U_{SHE}^{0} = U^{0} + \frac{RT}{nF} \ln \left(\frac{c_{ox}}{c_{red}}\right) \quad \text{Eqn 1}$$

where U is the cell potential, U_{SHE}^{0} is the potential of the standard hydrogen electrode, U^0 is the standard potential of the cell, R is the gas constant, T is the temperature, n is the number of electrons involved in the electron transfer reaction, F is Faraday's constant, C_{ox} is the concentration of the oxidized species, and C_{red} is the concentration of the reduced species. When the half-cycle is completed and the symmetric cell becomes under the open-circuit condition, the concentration of ions across the cell is once again allowed to equilibrate, and the cell potential decreases as a result. The potential between the beginning and end of the open-circuit period is, therefore, directly related to the mass transport of ions from the surface of the electrode. A larger potential drop is indicative of the accumulation of greater ions on the electrode surface, causing a larger concentration gradient in the cell.

Figure 6 shows the potential relaxations during open-circuit conditions after selected cycles for the Li, Na, organic Zn, and aqueous Zn symmetric cells. In each case, there is an increase in the potential drop during the open circuit period with an increased cycle number. The increased potential drops can be attributed to mass transport limitations. These limitations arise due to the buildup of "dead" metal on the surface of the electrode as well as the formation of solid-electrolyte interface (SEI) layers. The accumulation of the dead metal and the formation of SEI layers material create a tortuous path for ions to reach out the electrolyte (Figure 5E,F). Therefore, increasing the diffusion length lowers the effective diffusion coefficient in the electrolyte according to the equation

$$D_{eff} = D\frac{\epsilon}{\tau} \quad \text{Eqn 2}$$

where D_{eff} is the effective diffusion coefficient, D is the intrinsic diffusion coefficient, ε is the volume fraction of the conductive phase of the electrolyte, and τ is the tortuosity factor[37]. For each metal, the open circuit potential drop follows an exponential decay over the rest period. The shape of this decay arises from the movement of ions within the cell towards equilibrium conditions according to Fick's first law

$$J = -D_{eff}\frac{dc}{dx} \quad \text{Eqn 3}$$

where J is the mass flux of the metal ions, D_{eff} is the effective diffusion coefficient, c is the concentration of the metal ion, and x is the position in the direction perpendicular to the electrode surface. In cycle 1, the Li, Na, organic Zn, and aqueous Zn cells have a difference in potential of -2.76, -3.60, -14.3, and 0.15 mV, respectively, between the beginning and end of the open circuit relaxation period. The magnitude of these potential relaxations during the open circuit progressively increased for each symmetric cell until cell failure for all the organic cases. For the aqueous Zn cell, the drop in potential reaches a maximum of -2.70 V near cycle 150 before diminishing slightly over the remaining cycles. By the end of cycling, the total potential drops reached values of -28.3, -25.1, -24.5, and -2.33 mV for Li, Na, organic Zn, and aqueous zinc, respectively. The large potentials drops are only observed when the metal electrodes were cycled in the organic electrolyte. This observation further verifies the correlation between the accumulation of surface deposits on the metal electrode with transport limitations near the electrode surface.

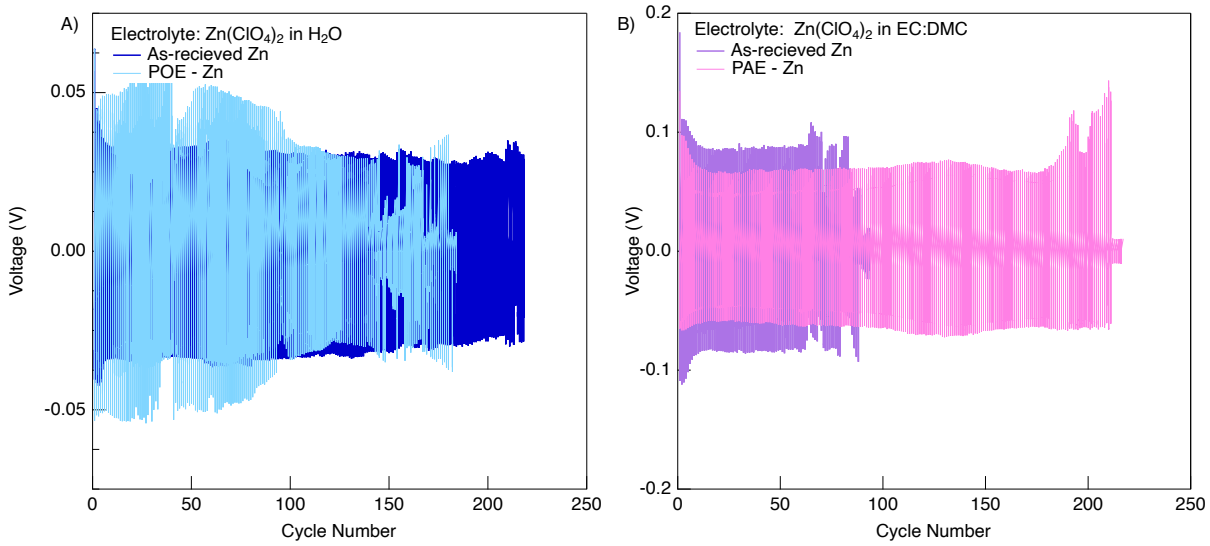

Figure 7: Voltage profiles for symmetrical cells during plating / stripping at $\pm$1 mA/cm^2 current density A) as-received zinc (dark blue) and POE-Zinc (light blue) cycled in aqueous electrolyte, B) as-received zinc (dark purple) and POE-Zinc (light pink) cycled in organic electrolyte.

3.2. Impact of Solid – Electrolyte Interface on Plating of Zn: The composition, thickness, and elasticity of the SEI layer on lithium and sodium electrode surfaces has a strong effect on the overpotentials during deposition/dissolution, long-term cycling stability, and plating/stripping Coulombic efficiencies[15,40,43]. Unlike Li and Na metal, Zn is compatible with organic and aqueous electrolytes which provides an opportunity to highlight the effects of organic SEI layers on deposition/dissolution behavior. XPS analysis (Fig S5) and SEM images (Fig 5) also indicates the thicker layer of SEI Formed in organic electrolytes compared to aqueous ones on Zinc electrodes. To elucidate the SEI effect on metal plating, in some cases, the symmetrical cells were pre-cycled in organic or aqueous electrolytes for 20 cycles. If the zinc electrode were pre-cycled in the organic electrolyte, these zinc electrodes are called as "POE-Zinc" where POE stands for Pre-cycled in Organic Electrolyte for twenty cycles. If the zinc electrode were pre-cycled in an aqueous electrolyte, these zinc electrodes are called as "PAE-Zinc" where PAO stands for Pre-cycled in Aqueous Electrolyte for twenty cycles. The resistance of the as-received Zn and PAE-zinc was compared by performing impedance measurements and the as-received zinc shows larger surface resistance compared to the PAE-zinc (Figure S6). The cells were made of zinc electrodes with

similar treatment as counter and working electrodes. For example, they are called as POE-Zinc cells if both electrodes were POE-Zinc electrodes.

The electrochemical performance of as-received zinc and the POE-Zinc were compared by cycling them in an aqueous electrolyte as shown in Figure 6A. The presence of the SEI layer formed in organic electrolyte during pre-cycling for 20 times contributed to higher overpotentials during the first 100 cycles in the POE-Zinc in aqueous electrolyte. Also, there is a maximum polarization in POE Zinc at cycle 45 is about 0.054 V. The overpotentials gradually decrease until the polarization in the POE-Zinc cell becomes similar with as-received zinc cycled in the aqueous electrolyte at around cycle 120. However, the POE-Zinc cell has a shorten cycle life and short-circuits at around 160 cycles compared to the as-received Zinc cell when cycled in an aqueous electrolyte.

Solid electrolyte interface has a complex morphology and chemistry. It undergoes serious changes by increasing charging / discharging time. Also, it proposed to have two distinct layers, where more inorganic compounds form near electrode interface and the SEI is composed of more organic species on the electrolyte interface[15]. In the case of aqueous electrolyte, the formation of SEI layer on the surface of the electrode is much thinner and it only composes of inorganic species due to decomposition of salt[44]. To differentiate the impact of a SEI layers formed in organic versus aqueous electrolytes, we also perform another set of experiments where asymmetrical Zinc cell is initially cycled in an aqueous electrolyte for 20 cycles, and then switched to the organic electrolyte. These cells were called as “the PAE-Zinc cell” . The electrochemical performance of PAE-Zinc is compared with as-received Zinc when they were cycled in organic electrolytes in Figure 6C and D. An initial pre-cycling in aqueous electrolyte produced an improvement in the performance of the PAE-Zinc in organic electrolyte. The maximum overpotential in PAE-Zinc cells (0.067 V) was lower than the one for as-received Zinc in organic electrolyte cells (0.088 V) at the cycle 45. PAE-Zinc cell short-circuited around cycle 230, however, the cycle life of as-received Zinc in the organic electrolyte is much less and it short-circuited around cycle 85. To understand the better performance of Zn cell when it is pre-cycled in aqueous electrolytes, we compare the potential profiles during Li plating and stripping.

***Fifth Charge*:** Figure 8 provides a comparison of the different Zn cells during the first half of the 5th cycle. PAE-Zinc cell presents a broadened initial peak shape and reduced overpotentials throughout the half-cycle in comparison with as-received Zinc in organic electrolytes. The broadened peak is accompanied by a shallower dip in voltage between the two peaks. The following voltage increase towards the second peak is greater in as-received Zn cell compared to the PAE-Zinc cell. Neither cell reaches a final plateau stage at the end of the half-cycle but is still increasing in overpotential when the half-cycle ends. POE-Zinc cell electrodes display a narrower peak at the beginning of the half-cycle than the as-received Zinc cell in aqueous electrolytes. The operational voltage of the POE-Zinc cell was almost 0.1 V greater than the as-received Zinc cell during the fifth charge cycle in aqueous electrolytes. Also, the voltage in the POE-Zinc cell demonstrates detectable noise, which could be related to the deformation of the organic SEI layers during the charge period. Overall, both cells produce comparable voltage trace shapes with an initial peak followed by a shallow dip in voltage before a final voltage increase.

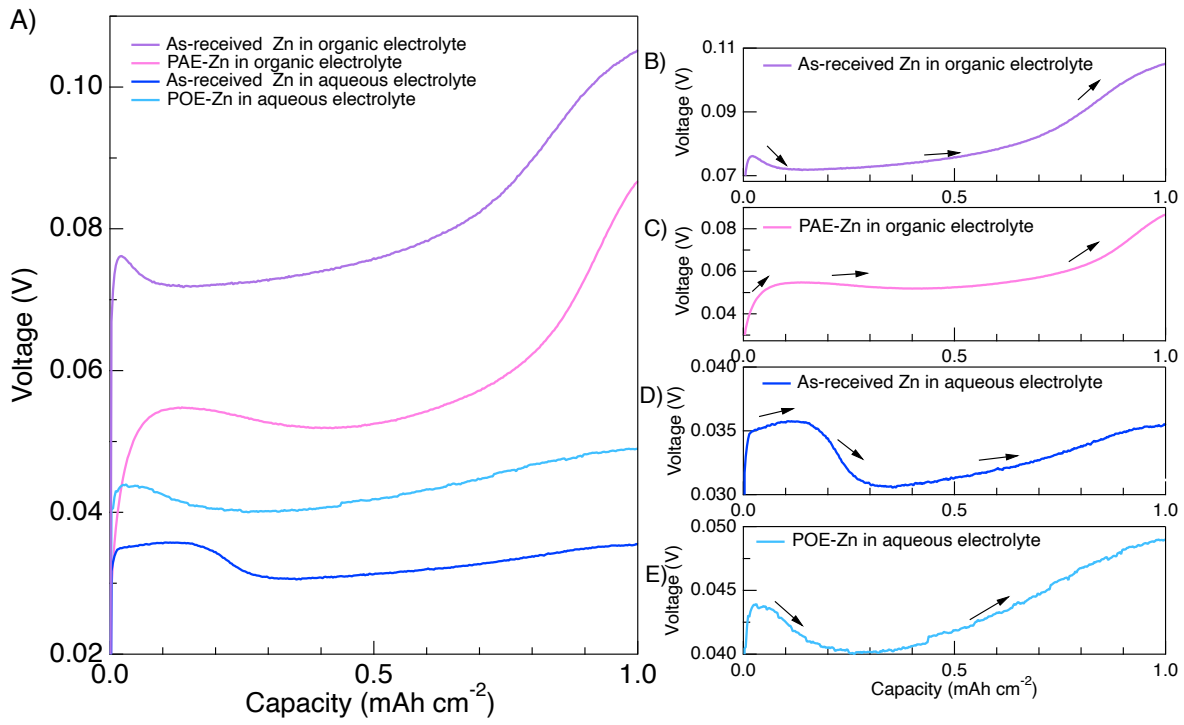

Figure 8: A) Fifth charge cycle voltage profiles at 1 mA cm^{-2}. B) As-received zinc (dark purple) and C) POE-Zinc (light pink) cycled in organic electrolyte; D) As-received zinc (dark blue) and E) POE-Zinc (light blue) cycled in aqueous electrolyte.

Later Cycles: Figure 9 shows the voltage profiles in the Zn symmetrical cells during 10th, 20th, 50th, 75th, 100th, 150th, and 200th cycles from Figure 7. As compared to the as-received Zn cell, the PAE-Zinc cell retains its voltage profile over more extended cycling in organic electrolytes. In the case of the cell containing as-received Zn electrodes, the voltage dip between the two maximums has largely disappeared by cycle 75; however, the voltage profile of the PAE-Zinc cell retains a small voltage dip even up to cycle 150. The dramatic voltage increases at the end of the later half-cycles of the as-received Zn cells are not present in the case of the PAE-Zinc cells at cycle number 75. PAE-Zinc cell eventually shows a large voltage increase during plating cycles, which shows similarity with the Li symmetrical cells in Figure 4. The increase in voltage is likely due to transport limitations associated with either accumulation of "dead" Zn on the surface or the formation of SEI layers in the organic electrolyte.

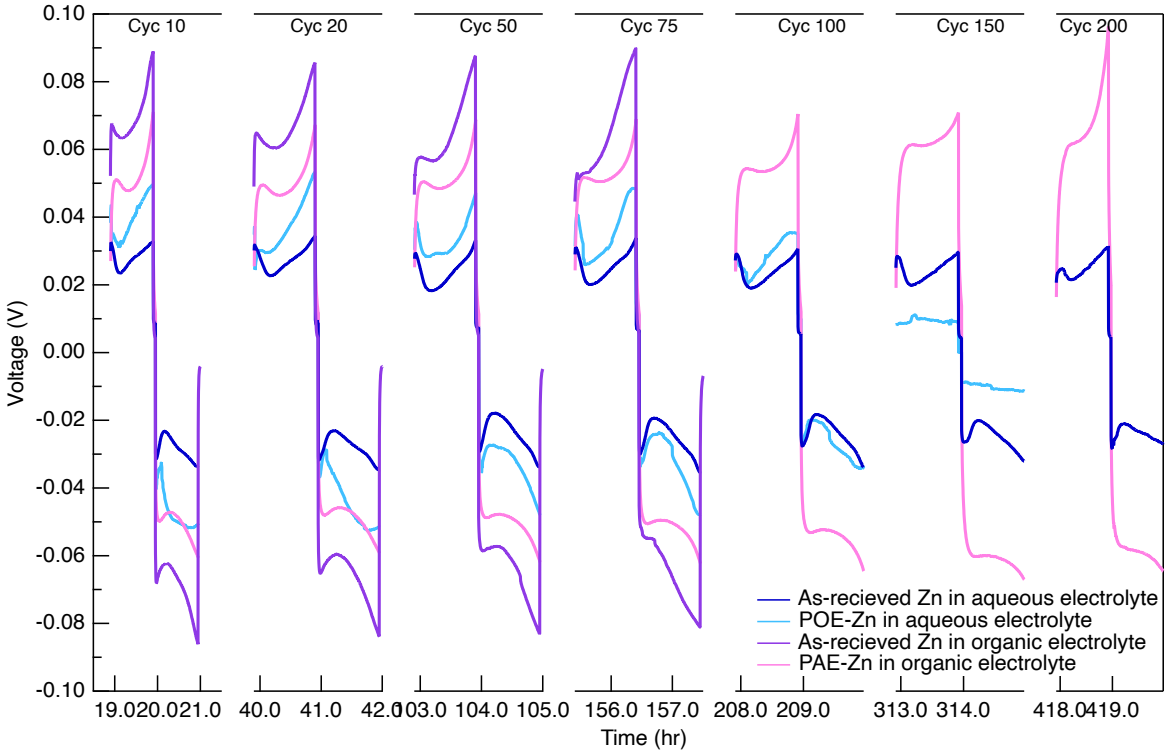

Figure 9: Galvanostatic cycling profiles symmetric cells charged / discharged at 1 mA cm^{-2}. As-received zinc (dark purple) and POE-Zinc (light pink) cycled in organic electrolyte; As-received zinc (dark blue) and E) POE-Zinc (light blue) cycled in aqueous electrolyte.

For the two aqueous Zn systems, extended cycling results in their voltage profiles becoming more alike. As described previously, the voltage trace of the cells made of as-received

Zn does not change substantially over long-term cycling. However, the voltage profile of the POE-Zinc cell does change noticeably over cycling and results in the growing similarity between the two. The presence of the SEI layer formed during the pre-cycle period in organic electrolytes contributes to increased overpotentials during the cycling in aqueous electrolytes These overpotentials reduce gradually until the voltage profile of the cell is made of as-received Zn and the cell made of PAE-Zinc cell begin to overlap by about cycle 100. However, the voltage demonstrates noise in the case of POE-Zinc cell.

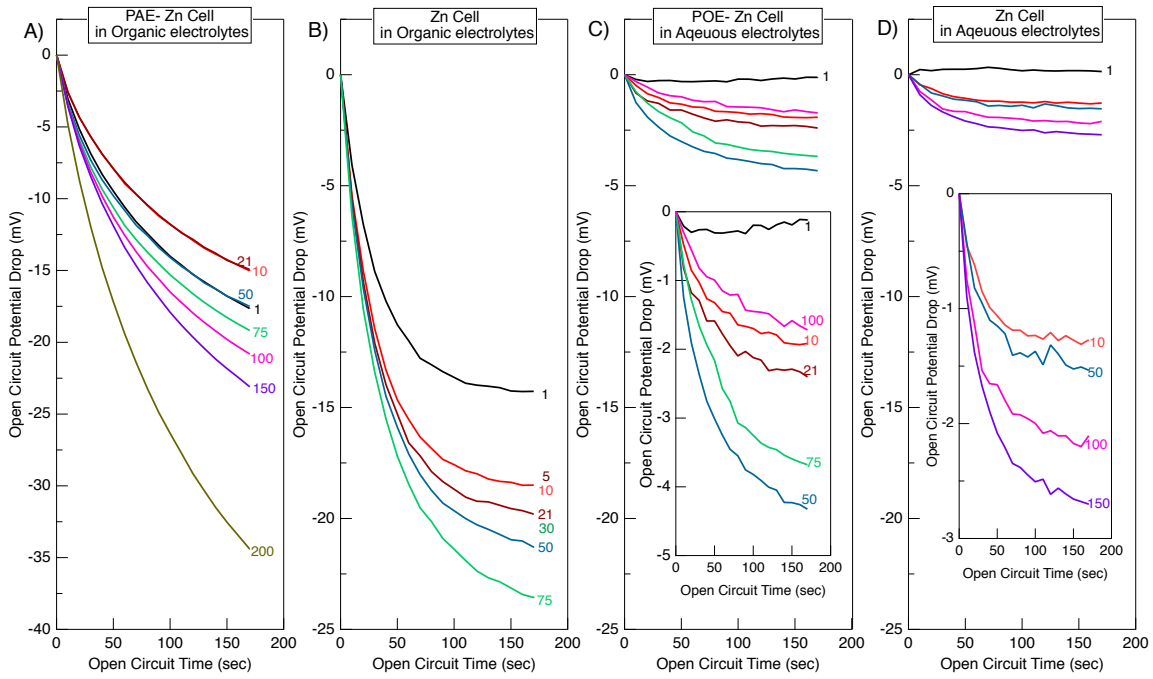

Figure 10: Open-circuit potential drops for selected cycles for As-received zinc and POE-Zinc cycled in organic electrolyte As-received zinc and POE-Zinc cycled in aqueous electrolyte

Open Circuit Potentials: Figure 10 shows the open circuit voltage drops for the symmetrical Zn cells cycled in either aqueous or organic electrolytes. The open-circuit potential dramatically dropped to almost 22.5 mV by cycle 75 in organic electrolytes for the cell made of as-received zinc electrodes. On the other hand, the open circuit potential drop initials reduced from 22.5 mV after the first cycle to 15 mV by cycle 10. Then, the open circuit potential drop gradually increased to 22.5 mV by the end of 150 cycles in organic electrolytes for the cell made of PAE-Zn electrodes. The cell demonstrated a sharp open circuit potential drop from 22.5 to 35 mV from cycle 150 to 200, respectively. This corresponds to the significant change in the voltage profile during plating

in Figure 9. For the aqueous electrolytes, the initial potential drop gradually rises to 4.1 mV by cycle 75, followed by a decrease to 1.58 mV by cycle 125 in POE-zinc cell. The potential drop behavior during the open circuit on POE-zinc cell suggests the deformation of the organic SEI layer between cycle numbers 75 and 125.

3.3. Discussion

In this study, we compared the cycling performance of Li, Na, and Zn symmetric cells using the same anionic salt (ClO_4^-) in the electrolyte solution. Zn metal enabled us to investigate the influence of organic SEI layers on electrochemical performance by allowing us to use both carbonate and aqueous electrolytes. These symmetric cells were evaluated by cycling at 1 mA/cm^2 up to an areal capacity of 1 mAh cm^{-2} with open circuit periods of 3 minutes in between each half-cycle. This revealed that the cycling lifetime of the different systems followed the order aqueous Zn>Li>organic Zn>Na. Additionally, a different failure mechanism was noted in the Na cell compared to the other systems. Whereas the aqueous Zn, organic Zn, and Li symmetric cells failed by short-circuiting over prolonged cycling, the Na symmetric cell failed due to a rapid rise in cell overpotential. This is likely due to the drying up of the electrolyte owing to Na's high reactivity with the electrolyte and the significant buildup of "dead" Na in the cell imposing mass transport limitations. Observations of the voltage traces revealed that organic Zn cells cycled in organic electrolytes exhibit similar voltage features as Li cells which can be correlated with deposition/dissolution processes occurring on the surface. Extended cycling revealed a switch from "peaking" to arcing voltage shapes for Li, Na, and Zn metals cycled in organic electrolytes. This observation agrees well with previous reports for Li and can be attributed to the buildup of a tortuous "dead" metal and SEI layer above the electrode surface which impedes metal ion diffusion and causes the cell's potential to switch from kinetically controlled to mass transport limited. The aqueous Zn cells showed much less pronounced changes in their voltage profile which is likely due to the absence of a porous organic SEI layer which would contribute to imposing mass transport limitations. Plots of the cell potential relaxations during the open circuit period after each half-cycle show an increase in potential drop for each of the four systems studied. The increase in potential relaxation can also be attributed to the buildup of a "dead" metal and SEI layer on the surface which increases the concentration gradient in the cell whenever a current is applied and slows relaxation of this potential gradient during the open circuit period. Notably, while the

organic cells reached large potential relaxations of ~ 20 mV before failure, the aqueous Zn cell only reached a value of ~2.5 mV which supports the notion that the aqueous Zn cell is less mass transport limited.

Further investigation of the role of an organic SEI layer on electrochemical performance in Zn cells was conducted by creating either an inorganic or organic SEI layer on the surface of Zn electrodes by cycling for 20 cycles in the aqueous or organic electrolyte, respectively. The electrolyte in the cell was then switched and electrochemical performance was evaluated. This procedure revealed that the presence of an SEI layer formed during pre-cycling in organic electrolytes increases cell polarization and reduced cycle life from ~225 cycles to ~160 cycles in aqueous electrolytes. Cell polarization in these cells gradually decreased and became more like the voltage traces of as-received Zn cells in aqueous electrolytes after extended cycling possibly indicating the breakdown of the organic SEI layer over time. A similar trend was noted in the potential relaxation drops during the open circuit period for the POE- Zn cells which had an increase in potential drop up to cycle 75 reaching a value of ~4 mV, but then experienced a decrease in potential drop for the remainder of cycling down to ~ 2 mV which agrees well with the potential drop in the as-received Zn cell in aqueous electrolyte. The presence of the SEI layer formed during pre-cycling in aqueous electrolytes greatly increased cell lifetime from about 90 cycles to about 230 cycles and also reduced cell overpotentials in organic electrolytes.

4. Conclusion

Electrochemical behavior of metal stripping and plating is compared for Li, Na and Zn cells in organic electrolytes using analogous salts and same solvent. These results demonstrate that similar correlations between voltage profiles and surface processes for Li and Na cells can be extended to describe Zn cells cycling in organic or aqueous electrolytes. Then, the impact of the SEI layer on the stripping / plating of Zn metal was investigated by performing series of electrochemical measurements using same salt dissolved in either organic or aqueous solvents. XPS, SEM and EIS measurements were conducted to analyze interfacial resistance and surface morphology of the Zinc electrodes. The study highlights the effects of the SEI layer formed during cycling in the organic electrolyte on cell performance and shows that the SEI layer forms in the organic electrolytes increases cell potentials and reduces cycle life in Zn cells. On the other hand, the thin layer of SEI formed in the aqueous electrolyte has a protective effect on the electrode during

plating and stripping cycles. In summary, zinc electrode offers a potential to elucidate the complex interfacial reactions during plating / stripping process because of its compatibility with organic and aqueous solvents.

5. Acknowledgment

We are grateful to the Oklahoma State University Start-up grant for supporting the research. The authors declare that they have no competing interests. SEM imaging in this work was conducting in the Oklahoma State University's Microscopy Laboratory and the equipment used was purchased through the NSF MRI program. The research was funded by the

6. References.

1. Li, M., Lu, J., Chen, Z. & Amine, K. 30 Years of Lithium-Ion Batteries. *Adv. Mater.* **30**, 1–24 (2018).

2. Thackeray, M. M., Wolverton, C. & Isaacs, E. D. Electrical energy storage for transportation - Approaching the limits of, and going beyond, lithium-ion batteries. *Energy Environ. Sci.* **5**, 7854–7863 (2012).

3. Whittingham, M. S. Ultimate Limits to Intercalation Reactions for Lithium Batteries. *Chem. Rev.* **114**, 11683–11720 (2014).

4. Xu, W. *et al.* Lithium metal anodes for rechargeable batteries. *Energy Environ. Sci.* **7**, 513–537 (2014).

5. Seh, Z. W., Sun, J., Sun, Y. & Cui, Y. A highly reversible room-temperature sodium metal anode. *ACS Cent. Sci.* **1**, 449–455 (2015).

6. Chazalviel, J. N. Electrochemical aspects of the generation of ramified metallic electrodeposits. *Phys. Rev. A* **42**, 7355–7367 (1990).

7. Aurbach, D., Zinigrad, E., Yaron, C. & Hanan, T. A short review of failure mechanisms of lithium metal and lithiated graphite anodes in liquid electrolyte solutions. *Solid State Ionics* **148**, 405–416 (2002).

8. Xu, K. Electrolytes and interphases in Li-ion batteries and beyond. *Chem. Rev.* **114**, 11503–11618 (2014).

9. Peled, E. The Electrochemical Behavior of Alkali and Alkaline Earth Metals in Nonaqueous Battery Systems—The Solid Electrolyte Interphase Model. *J. Electrochem. Soc.* **126**, 2047 (1979).

10. Cohen, Y. S., Cohen, Y. & Aurbach, D. Micromorphological studies of lithium electrodes in alkyl carbonate solutions using in situ atomic force microscopy. *J. Phys. Chem. B* **104**, 12282–12291 (2000).

11. Steiger, J., Kramer, D. & Mönig, R. Microscopic observations of the formation, growth, and shrinkage of lithium moss during electrodeposition and dissolution. *Electrochim. Acta*

136, 529–536 (2014).

12. Yoshimatsu, I., Hirai, T. & Yamaki, J. Lithium Electrode Morphology during Cycling in Lithium Cells. *J. Electrochem. Soc.* **135**, 2422–2427 (1988).

13. Mandl, M. *et al.* Sodium metal anodes: Deposition and dissolution behavior and SEI formation. *Electrochim. Acta* **354**, 136698 (2020).

14. Fang, C. *et al.* Quantifying inactive lithium in lithium metal batteries. *Nature* **572**, 511–515 (2019).

15. He, M., Guo, R., Hobold, G. M., Gao, H. & Gallant, B. M. The intrinsic behavior of lithium fluoride in solid electrolyte interphases on lithium. *Proc. Natl. Acad. Sci. U. S. A.* **117**, 73–79 (2020).

16. Chen, L. *et al.* Novel ALD Chemistry Enabled Low-Temperature Synthesis of Lithium Fluoride Coatings for Durable Lithium Anodes. *ACS Appl. Mater. Interfaces* **10**, 26972–26981 (2018).

17. Li, N. W., Yin, Y. X., Yang, C. P. & Guo, Y. G. An Artificial Solid Electrolyte Interphase Layer for Stable Lithium Metal Anodes. *Adv. Mater.* **28**, 1853–1858 (2016).

18. Zhao, Y. *et al.* In situ formation of highly controllable and stable Na 3 PS 4 as a protective layer for Na metal anode. *J. Mater. Chem. A* **7**, 4119–4125 (2019).

19. Liu, M. *et al.* Artificial Solid-Electrolyte Interface Facilitating Dendrite-Free Zinc Metal Anodes via Nanowetting Effect. *ACS Appl. Mater. Interfaces* **11**, 32046–32051 (2019).

20. Zhang, X. Q., Cheng, X. B., Chen, X., Yan, C. & Zhang, Q. Fluoroethylene Carbonate Additives to Render Uniform Li Deposits in Lithium Metal Batteries. *Adv. Funct. Mater.* **27**, 1–8 (2017).

21. Wang, G. *et al.* Suppressing dendrite growth by a functional electrolyte additive for robust Li metal anodes. *Energy Storage Mater.* **23**, 701–706 (2019).

22. Komaba, S. *et al.* Fluorinated ethylene carbonate as electrolyte additive for rechargeable Na batteries. *ACS Appl. Mater. Interfaces* **3**, 4165–4168 (2011).

23. Lee, B., Paek, E., Mitlin, D. & Lee, S. W. Sodium Metal Anodes: Emerging Solutions to

Dendrite Growth. *Chem. Rev.* (2019) doi:10.1021/acs.chemrev.8b00642.

24. Banik, S. J. & Akolkar, R. Suppressing Dendritic Growth during Alkaline Zinc Electrodeposition using Polyethylenimine Additive. *Electrochim. Acta* **179**, 475–481 (2015).

25. Zhou, W. *et al.* Plating a Dendrite-Free Lithium Anode with a Polymer/Ceramic/Polymer Sandwich Electrolyte. *J. Am. Chem. Soc.* **138**, 9385–9388 (2016).

26. Chen, L. *et al.* PEO/garnet composite electrolytes for solid-state lithium batteries: From "ceramic-in-polymer" to "polymer-in-ceramic". *Nano Energy* **46**, 176–184 (2018).

27. Zhou, W., Li, Y., Xin, S. & Goodenough, J. B. Rechargeable Sodium All-Solid-State Battery. *ACS Cent. Sci.* **3**, 52–57 (2017).

28. Zhao, N. *et al.* Flexible Hydrogel Electrolyte with Superior Mechanical Properties Based on Poly(vinyl alcohol) and Bacterial Cellulose for the Solid-State Zinc-Air Batteries. *ACS Appl. Mater. Interfaces* **11**, 15537–15542 (2019).

29. Zuo, T. T. *et al.* Graphitized Carbon Fibers as Multifunctional 3D Current Collectors for High Areal Capacity Li Anodes. *Adv. Mater.* **29**, 1–6 (2017).

30. Wang, Z. *et al.* Conducting Polymer Paper-Derived Mesoporous 3D N-doped Carbon Current Collectors for Na and Li Metal Anodes: A Combined Experimental and Theoretical Study. *J. Phys. Chem. C* **122**, 23352–23363 (2018).

31. An, Y. *et al.* Heteroatom-doped 3D porous carbon architectures for highly stable aqueous zinc metal batteries and non-aqueous lithium metal batteries. *Chem. Eng. J.* **400**, (2020).

32. Maraschky, A. & Akolkar, R. Mechanism Explaining the Onset Time of Dendritic Lithium Electrodeposition via Considerations of the Li + Transport within the Solid Electrolyte Interphase. **165**, 696–703 (2018).

33. Aleshin, A., Bravo, S., Request, K. & Wood, K. N. Rapid oxidation and reduction of lithium for improved cycling performance and increased homogeneity. *ACS Appl. Mater. Interfaces* **13**, 2654–2661 (2021).

34. Sanchez, A. J. *et al.* Plan-View Operando Video Microscopy of Li Metal Anodes:

Identifying the Coupled Relationships among Nucleation, Morphology, and Reversibility. *ACS Energy Lett.* (2020) doi:10.1021/acsenergylett.0c00215.

35. Wood, K. N., Noked, M. & Dasgupta, N. P. Lithium metal anodes: Toward an improved understanding of coupled morphological, electrochemical, and mechanical behavior. *ACS Energy Letters* vol. 2 (2017).

36. Wood, K. N. *et al.* Dendrites and pits: Untangling the complex behavior of lithium metal anodes through operando video microscopy. *ACS Cent. Sci.* **2**, 790–801 (2016).

37. Chen, K. H. *et al.* Dead lithium: Mass transport effects on voltage, capacity, and failure of lithium metal anodes. *J. Mater. Chem. A* **5**, 11671–11681 (2017).

38. Özdogru, B., Dykes, H., Padwal, S., Harimkar, S. & Çapraz, Ö. Electrochemical strain evolution in iron phosphate composite cathodes during lithium and sodium ion intercalation. *Electrochim. Acta* **353**, (2020).

39. Ding, F. *et al.* Effects of Carbonate Solvents and Lithium Salts on Morphology and Coulombic Efficiency of Lithium Electrode. *J. Electrochem. Soc.* **160**, A1894–A1901 (2013).

40. Bieker, G., Winter, M. & Bieker, P. Electrochemical in situ Investigations of SEI and dendrite formation on the lithium metal anode. *Phys. Chem. Chem. Phys.* **17**, 8670–8679 (2015).

41. Behavior, M., Wood, K. N., Noked, M. & Dasgupta, N. P. Lithium Metal Anodes : Toward an Improved. (2017) doi:10.1021/acsenergylett.6b00650.

42. Fuller, T. & Harb, J. *Electrochemical Engineering*. (John Wiley and Sons Inc., 2018).

43. Iermakova, D. I., Dugas, R., Palacín, M. R. & Ponrouch, A. On the Comparative Stability of Li and Na Metal Anode Interfaces in Conventional Alkyl Carbonate Electrolytes. *J. Electrochem. Soc.* **162**, A7060–A7066 (2015).

44. Fu, J. *et al.* Electrically Rechargeable Zinc-Air Batteries: Progress, Challenges, and Perspectives. *Adv. Mater.* **29**, (2017).